Solar Phys (2017) 292:65
DOI 10.1007/s11207-017-1080-9

Estimation of Reconnection Flux Using Post-eruption Arcades and Its Relevance to Magnetic Clouds at 1 AU

N. Gopalswamy[1] · **S. Yashiro**[2] · **S. Akiyama**[2] · **H. Xie**[2]

Received: 24 September 2016 / Accepted: 14 March 2017 / Published online: 10 April 2017
© Springer Science+Business Media Dordrecht (outside the USA) 2017

Abstract We report on a new method to compute the flare reconnection (RC) flux from post-eruption arcades (PEAs) and the underlying photospheric magnetic fields. In previous works, the RC flux has been computed using the cumulative flare ribbon area. Here we obtain the RC flux as the flux in half of the area underlying the PEA in EUV imaged after the flare maximum. We apply this method to a set of 21 eruptions that originated near the solar disk center in Solar Cycle 23. We find that the RC flux from the arcade method (Φ_{rA}) has excellent agreement with the flux from the flare-ribbon method (Φ_{rR}) according to $\Phi_{\mathrm{rA}} = 1.24(\Phi_{\mathrm{rR}})^{0.99}$. We also find Φ_{rA} to be correlated with the poloidal flux (Φ_{P}) of the associated magnetic cloud at 1 AU: $\Phi_{\mathrm{P}} = 1.20(\Phi_{\mathrm{rA}})^{0.85}$. This relation is nearly identical to that obtained by Qiu *et al.* (*Astrophys. J.* **659**, 758, 2007) using a set of only 9 eruptions. Our result supports the idea that flare reconnection results in the formation of the flux rope and PEA as a common process.

Keywords Coronal mass ejections · Flares · Flux rope · Magnetic cloud, reconnection flux

1. Introduction

A number of investigations have identified a close connection between coronal mass ejections (CMEs) and the associated flares: i) the CME acceleration is synchronized with the rise time of the associated flare (Zhang *et al.*, 2001; Zhang and Dere, 2006; Gopalswamy *et al.*, 2012), ii) the CME kinetic energy and soft X-ray peak flux are correlated (Gopalswamy, 2009), iii) the CME width is determined by the flare magnetic field (Moore, Sterling, and Suess, 2007), iv) flare reconnection (RC) and flux rope formation are related (Leamon *et al.*, 2004; Longcope and Beveridge, 2007; Qiu *et al.*, 2007;

Earth-affecting Solar Transients
Guest Editors: Jie Zhang, Xochitl Blanco-Cano, Nariaki Nitta, and Nandita Srivastava

✉ N. Gopalswamy
nat.gopalswamy@nasa.gov

[1] NASA Goddard Space Flight Center, Greenbelt, MD, USA

[2] The Catholic University of America, Washington, DC, USA

Hu *et al.*, 2014), v) the CME nose is directly above the flare location (Yashiro *et al.*, 2008), and vi) the high charge state of minor ions in interplanetary coronal mass ejections (ICMEs) is a consequence of the heated flare plasma entering the CME flux rope during the eruption (Lepri *et al.*, 2001; Reinard, 2008; Gopalswamy *et al.*, 2013a). One of the key aspects of CMEs is their flux rope nature, which has been considered extensively from theory and observations (see *e.g.*, Mouschovias and Poland, 1978; Burlaga *et al.*, 1981; Marubashi, 1997; Gibson *et al.*, 2006; Linton and Moldwin, 2009). The flux rope nature of CMEs provides an important eruption scenario that can be tested using remote-sensing and *in-situ* observations.

A number of investigations have also shown that the flare RC process results in the simultaneous formation of a post-eruption arcade (PEA) and a flux rope during solar eruptive events (Leamon *et al.*, 2004; Longcope and Beveridge, 2007; Qiu *et al.*, 2007; Hu *et al.*, 2014). At present, it is not fully understood whether CME flux ropes exist before eruption or if they are formed during eruption. The reality may be something in between: flux may be added to a pre-existing flux rope via flare RC (see *e.g.*, Lin, Raymond, and van Ballegooijen, 2004). If the flux rope is formed by reconnection, the flux rope is twisted by one turn for each flare loop that forms, as explained in Longcope *et al.* (2007); Longcope and Beveridge (2007). The flare loops are rooted in the flare ribbons on either side of the polarity inversion line. Thus flare reconnection flux Φ_{r} and the poloidal flux Φ_{p} of the associated flux rope at 1 AU are expected to be equal. On the other hand, $\Phi_{\mathrm{r}} < \Phi_{\mathrm{p}}$ might indicate that flux is added to preexisting flux of the flux rope. For a set of nine eruptions, Qiu *et al.* (2007) computed Φ_{r} from the *Transition Region and Coronal Explorer* (TRACE: Strong *et al.*, 1994) 1600 Å flare-ribbon areas and photospheric/chromospheric magnetic field strength. They compared Φ_{r} with Φ_{p} obtained by fitting a flux rope to the *in-situ* observations of the associated CMEs and found an approximate equality between Φ_{r} and Φ_{p}. Qiu *et al.* (2007) analysis resulted in the relation

$$\Phi_{\mathrm{p}} = 1.12(\Phi_{\mathrm{r}})^{0.82}, \tag{1}$$

suggesting that Φ_{r} is approximately equal to Φ_{p}. One of the reasons for the small number of events is that complete observations of flare ribbons are rare. The purpose of this article is to report on a new technique to compute Φ_{r} from PEAs and also to test the Φ_{r}–Φ_{p} relationship with a larger data set.

2. Description of the New Technique and Data

The post-eruption arcade (PEA) technique to determine Φ_{r} makes use of the close relationship between flare ribbons and PEAs because the ribbons essentially mark the footprints of PEAs. Instead of counting the ribbon pixels in a series of images, we demarcate the area under PEAs, A_{P}, using a polygon, overlplot the polygon on a magnetogram obtained around the time of the PEA image, and sum the absolute value of the photospheric magnetic flux in all the pixels within the polygon. The resulting RC flux is then half of the total flux through the polygon. The justification for this technique is that the ribbon separation ends after the flare maximum and the accumulated pixel area should roughly correspond to the area below the PEA on one side of the polarity inversion line.

2.1. Illustrative Examples

As an example we consider the 12 May 1997 eruption, which resulted in a magnetic cloud (MC) detected by the *Wind* and *Advance Composition Explorer* (ACE) spacecraft (Gopalswamy *et al.*, 2010). The eruption occurred in NOAA Active Region (AR) 8038 located at N21W08. Various aspects of this event have been studied extensively using remote observations (Thompson *et al.*, 1998; Webb *et al.*, 2000), *in-situ* observations (Baker *et al.*, 1998), and modeling (Titov *et al.*, 2008). Figure 1 shows the evolution of the eruption in a series of Hα pictures from the *Domeless Solar Tower Telescope* of the Kyoto University's Hida Observatory in Japan (Nakai and Hattori, 1985) revealing the evolution of the flare ribbons. Initially, the ribbons are thin and close to each other. As time progresses, the ribbons separate and their areas increase. The RC flux in the ribbons is the magnetic flux computed over the cumulative area of the ribbons on one side of the polarity inversion line (PIL) in the flaring region. Ideally, the ribbons are well defined over the whole event and either side of the PIL can be used. In practice, the ribbons can have different morphology on either side of the PIL. If the measurements are from both sides of the ribbon, we divided the flux by two. Sometimes, we were able to measure the area only from one side of the PIL. In computing the cumulative area, we eliminated the overlapping area in successive frames to avoid double counting. In the case of the 12 May 1997 event, both ribbons are well defined, so that we computed the total cumulative area below both ribbons. The outline of the cumulative ribbon areas are superposed on a magnetogram obtained by the *Michelson Doppler Imager* (MDI: Scherrer *et al.*, 1995) onboard the *Solar and Heliospheric Observatory* (SOHO: Domingo, Fleck, and Poland, 1995), as shown in Figure 1. The cumulative ribbon area was 1.7×10^{19} cm^2 (both ribbons) and the average field strength was 171.5 G. The RC flux corresponds to the flux in one ribbon, which means that we obtain an average $\Phi_{\mathrm{rR}} = 1.46 \times 10^{21}$ Mx. We denote the RC flux from the ribbon method by Φ_{rR} to distinguish it from the flux obtained using the arcade method (Φ_{rA}).

In order to compute Φ_{rA}, we consider a 195 Å EUV image at 16:50 UT obtained by the *Extreme-ultraviolet Imaging Telescope* (EIT: Delaboudiniére *et al.*, 1995) onboard SOHO. By visual examination, we marked the edges of the PEA as a polygon, which we superposed on an MDI magnetogram obtained at 16:04 UT (see Figure 2). The flux in each MDI pixel within the polygon is summed to obtain the total flux in the arcade area as 4.72×10^{21} Mx. Half of this quantity is the flare RC flux from the arcade method, $\Phi_{\mathrm{rA}} = 2.36 \times 10^{21}$ Mx. We see that Φ_{rA} is larger than Φ_{rR} by 38%. Given the uncertainties in identifying the edges of the ribbons, the agreement is reasonable.

Since there were not many events with good Hα flare observations, we also considered flare ribbons observed with TRACE at 1600 Å. Figure 3 shows an event with PEAs from SOHO/EIT 195 Å and TRACE 171 Å, while the ribbons are from TRACE 1600 Å. The eruption is the famous Bastille Day (14 July 2000) event, which had severe space weather impact because of a large solar energetic particle event that included ground-level enhancement (Gopalswamy *et al.*, 2004; Gopalswamy *et al.*, 2012; Mewaldt *et al.*, 2012) and a super-intense geomagnetic storm (Zhang *et al.*, 2007). Various aspects of this eruption have been extensively studied (Reiner *et al.*, 2001; Aschwanden and Alexander, 2001; Yan and Huang, 2003 and references therein). As in Figure 1, we mark the PEA area by a polygon drawn on the SOHO/EIT 195 Å image. The TRACE image has a spatial resolution of ~ 1 arcsec compared to ~ 5 arcsec in the EIT image, which is evident in the detailed structure of the arcade in the TRACE image. We also see some difference at the edges of the arcade, where TRACE observes additional faint structures. Despite this difference, we use the EIT images for identifying the arcade area because they are full-disk images and hence most of the eruptions are observed. Furthermore, not all arcades were observed by TRACE because of its limited FOV, and it was generally pointed at intense flaring regions. The RC flux estimated from the EIT area of the arcade and the MDI pixels within the area gives a flux of 13.1×10^{21} Mx. The additional structures to the right edge of the polygon contribute only $\sim 5.2 \times 10^{19}$ Mx, which is only about 0.4% of the arcade flux and hence negligible.

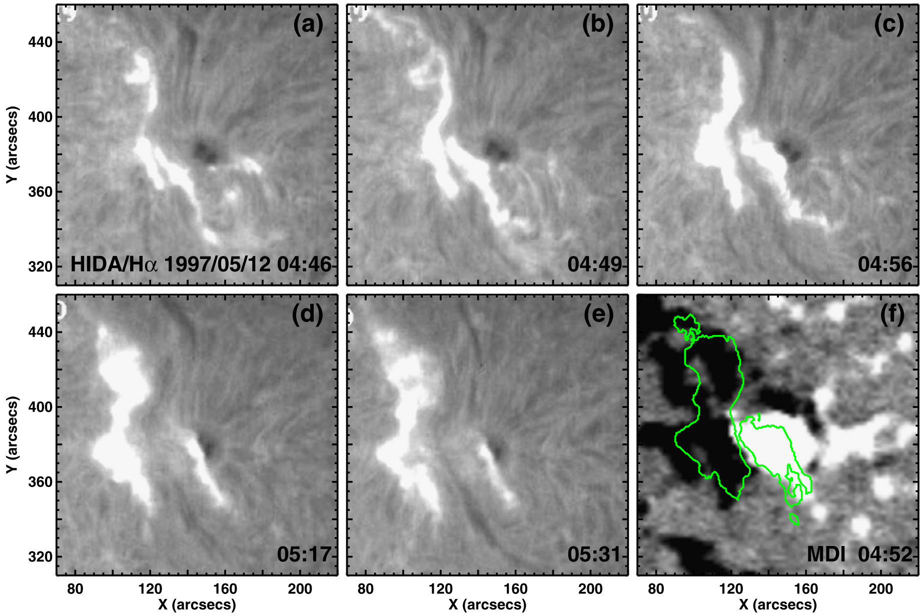

Figure 1 A series of Hα images (a – e) from the Hida Observatory of Kyoto University in Japan showing flare ribbons for the 12 May 1997 (event 2) eruption from 04:46 to 05:31 UT. The cumulative ribbon areas denoted by the green contours in panel (f) are superposed on an MDI magnetogram obtained at 04:52 UT (white is the positive and black is the negative magnetic field in the magnetogram). The total ribbon area is 1.7×10^{19} cm^2. With the average field strength of 171.5 G within the ribbon area, the RC flux becomes 1.46×10^{21} Mx (average below one ribbon).

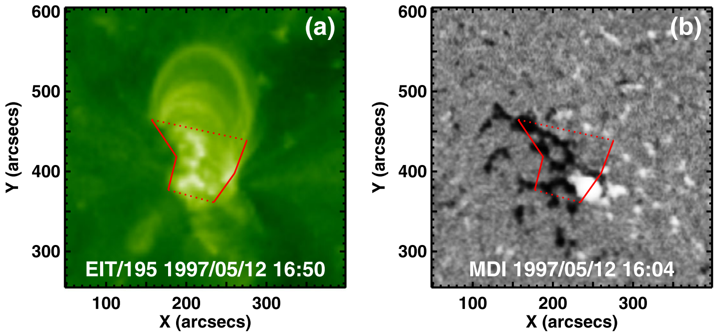

Figure 2 (a) The post-eruption arcade imaged by SOHO/EIT at 195 Å at 16:50 UT for the 12 May 1997 (event 2) eruption. The solid lines are drawn near the feet of the arcade, while the dashed lines complete the polygon. The EUV images have a pixel size of ∼2.6 arcsec. (b) The polygon from panel (a) is superposed on an MDI magnetogram at 16:04 UT. Summing the flux from each pixel within the area occupied by the arcade (corrected for projection effects) and dividing by two, we obtain the total flux as 2.36×10^{21} Mx (the arcade area is 4.25×10^{19} cm^2).

Figure 3 also shows that the ribbon is very extensive and well defined for measurements of the RC flux from flare ribbons. We used 71 of the 381 TRACE 1600 Å images available between 10:00 UT and 14:59 UT to obtain the ribbon area as 5.64×10^{19} cm^2. The average

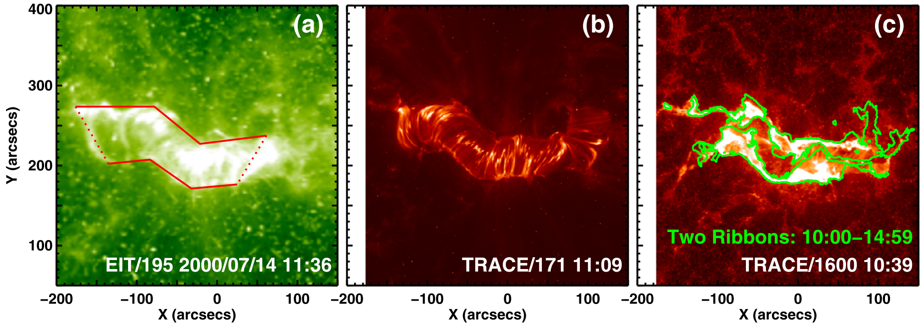

Figure 3 PEA of the 14 July 2000 (event 19) eruption as observed by (a) SOHO/EIT at 195 Å and (b) TRACE at 171 Å. The TRACE image in panel (c) taken at 10:39 UT shows the ribbons at 1600 Å. The green contour in (c) corresponds to the cumulative ribbon area (TRACE 1600 Å) between 10:00 and 14:59 UT.

magnetic field strength below the ribbon area was 446.9 G. The average RC flux from the ribbons on one side of the neutral line was obtained as 12.61×10^{21} Mx. This value is also close to the RC flux from the arcade method, differing only by $\sim 3.7\%$. We note that the RC flux in the 14 July 2000 event is much higher than the flux in the 12 May 1997 event because of the high magnetic field strength. Only one Hα image at 10:03 UT was available for this event. The ribbon area was 1.69×10^{19} cm^2 and the average field strength was 557.5 G, giving a partial RC flux of 9.44×10^{21} Mx, which is an underestimate, but consistent with the RC flux from the arcade method.

2.2. The Data Set

We are interested in solar eruptions that result in an MC at Earth so that we can make quantitative comparison between the flare RC flux and the poloidal flux of the associated MCs. For this purpose, we started with the list of 54 eruptions in Solar Cycle 23 considered for the Flux Rope CDAW workshops (Gopalswamy *et al.*, 2013b). The eruptions occurred from within $\pm 15^\circ$ in longitude from the disk center. The longitudinal criterion was imposed to ensure that the associated CMEs observed by the *Large Angle and Spectrometric Coronagraph* (LASCO: Brueckner *et al.*, 1995) arrived at Earth as interplanetary CMEs (ICMEs), as detected *in situ* by spacecraft located at Sun–Earth L1. The PEAs in the eruptions were observed in EUV or X-rays, and their measurable properties have already been reported (*e.g.*, Yashiro *et al.*, 2013). Yashiro and colleagues compared PEAs associated with CMEs that ended up at 1 AU as MCs and non-cloud ICMEs. We are interested in MCs because their flux rope structure allows us to determine the poloidal flux of the MCs at 1 AU (*e.g.*, Lepping, Burlaga, and Jones, 1990) to compare them with the RC flux. The fitted parameters of the MCs are available online (http://wind.nasa.gov/mfi/mag_cloud_S1.html).

Of the 54 ICMEs, only 23 were MCs. For one of the MCs, there was no EIT observations. For another event, the arcade at the Sun was not well defined. Excluding these two events, we have listed the remaining 21 events in Table 1. The event number (column 1) is taken from the CDAW list (Gopalswamy *et al.*, 2013a). We have retained the original event identifiers to facilitate comparison. The date and time of the MC and the associated CME at the Sun are listed in columns 2 and 3, respectively. The start time of the associated soft X-ray flare, the flare class, and the flare location in heliographic coordinates are listed in columns 4, 5, and 6, respectively. The area below the EUV arcade (A_a in units of 10^{19} cm^2, column 7),

Table 1 List of solar eruptions that were associated with magnetic clouds at Earth.

No	MC Date UT	CME Date UT	Flare UT	Class	Loc.	A_a	$\langle B_a \rangle$	Φ_{rA}	A_R	$\langle B_R \rangle$	Φ_{rR}	Φ_p
02	1997/05/15 01:15	SOL1997-05-12T05:30	04:42	C1.3	N21W08	4.25	111.1	2.36	1.70^{H}	171.5	1.46	4.06
09	1999/04/16 11:10	SOL1999-04-13T03:30	01:45	B4.3	N16E00	10.38	28.1	1.46	2.06^{aH}	46.8	0.48	4.94
16	2000/02/20 21:00	SOL2000-02-17T21:30	20:17	M1.3	S29E07	5.57	107.4	2.99	3.24^{H}	138.6	2.25	4.52
19	2000/07/15 14:18	SOL2000-07-14T10:54	10:03	X5.7	N22W07	7.50	349.4	13.10	5.64^{TaH}	446.9	12.61	13.52
21	2000/07/28 06:39	SOL2000-07-25T02:43	02:43	M8.0	N06W08	0.93	240.9	1.13	0.82^{T}	310.3	1.27	1.90
23	2000/08/11 18:51	SOL2000-08-09T16:30	15:19	EP	N20E12	7.21	172.0	6.20	–	–	–	8.10
24	2000/09/17 17:00	SOL2000-09-16T05:18	04:06	M5.9	N14W07	3.72	298.1	5.55	–	–	–	7.96
26	2000/10/12 22:36	SOL2000-10-09T23:50	23:19	C6.7	N01W14	15.94	64.0	5.10	3.08^{aH}	125.1	1.93	2.90
27	2000/11/06 09:20	SOL2000-11-03T18:26	18:35	C3.2	N02W02	35.85	113.5	20.35	–	–	–	6.16
32	2001/04/11 16:19	SOL2001-04-10T05:30	05:06	X2.3	S23W09	7.34	194.9	7.15	5.75^{H+T}	299.9	8.62	4.86
33	2001/04/28 05:02	SOL2001-04-26T12:30	11:26	M1.5	N20W05	16.45	145.9	12.00	3.86^{aH}	167.2	6.45	2.50
36	2002/03/18 13:13	SOL2002-03-15T23:06	22:09	M2.2	S08W03	12.46	183.8	11.45	1.18^{aH}	363.1	4.28	3.08
37	2002/04/17 11:01	SOL2002-04-15T03:50	03:05	M1.2	S15W01	4.78	452.1	10.80	0.81^{H}	1137.1	4.58	4.80
39	2002/05/18 19:51	SOL2002-05-16T00:50	00:11	C4.5	S23E15	8.36	113.2	4.74	–	–	–	8.88

Table 1 (*Continued*)

No	MC Date UT	CME Date UT	Flare UT	Class	Loc.	A_a	$\langle B_a \rangle$	Φ_{rA}	A_R	$\langle B_R \rangle$	Φ_{rR}	Φ_p
43	2002/08/01 05:10	SOL2002-07-29T12:07	10:27	M4.7	S10W10	2.40	511.5	6.15	0.64^{aT}	426.4	1.35	1.83
44	2003/08/17 13:40	SOL2003-08-14T20:06	17:12	wave	S10E02	4.16	522.1	10.85	–	–	–	4.36
45	2003/10/29 06:00	SOL2003-10-28T11:30	11:00	X17.2	S16E08	11.94	347.5	20.75	7.05^{T}	592.1	20.88	25.32
46	2003/10/30 16:20	SOL2003-10-29T20:54	20:37	X10.0	S15W02	8.71	496.1	21.60	3.96^{TaH}	698.4	13.82	7.58
49	2004/11/09 09:05	SOL2004-11-06T02:06	01:40	M3.6	N09E05	4.12	325.5	6.70	0.98^{H+T}	1009.8	4.93	6.06
53	2005/05/15 02:19	SOL2005-05-13T17:12	16:13	M8.0	N12E11	4.88	274.8	6.70	4.06^{H+T}	353.6	7.19	20.24
54	2005/05/20 03:34	SOL2005-05-17T03:26	02:31	M1.8	S15W00	2.45	210.6	2.58	–	–	–	2.22

Notes.

Flare date is the same as the CME date.

Below the flare class: EP = eruptive prominence, wave = EUV wave.

A_a – Area below the post-eruption arcade in 10^{19} cm^2.

$\langle B_a \rangle$ – average photospheric magnetic field strength (G) below the arcade.

Φ_{rA} – RC flux (in 10^{21} Mx) obtained from the arcade method (half of the flux passing through area A_a).

A_R – Cumulative ribbon area (in 10^{19} cm^2) from Hα or TRACE 1600 Å observations.

$\langle B_R \rangle$ – average photospheric magnetic field strength (G) below the cumulative ribbon area.

Φ_{rR} – RC flux (in 10^{21} Mx) obtained from the ribbon method.

Φ_p – Poloidal flux (in 10^{21} Mx) of the magnetic cloud at 1 AU in 10^{19} cm^2.

Superscript H – complete Hα observations.

Superscript T – complete TRACE observations.

Superscript aH – incomplete Hα observations.

Superscript aT – incomplete TRACE observations.

Superscript H + T – Complete Hα and TRACE ribbon observations; combined Hα and TRACE information listed.

Superscript TaH – Complete TRACE and incomplete Hα ribbon observation; TRACE information listed.

the average field strength (B_a in Gauss, in column 8) and half of the total unsigned magnetic flux below the arcade (Φ_{rA} in units of 10^{21} Mx, column 9) are derived with the PEA method described in Figures 1 and 2. Hα observations were generally not uniform and were also not available for many events. In some cases, we were able to measure the ribbon area only on one side of the neutral line. In some cases, only a single frame of the Hα image was available; the ribbon area in such cases represents a lower limit to the area. In all, there was at least one Hα picture for 12 events. Of these, only eight had more than one Hα frames; the number of frames were sufficient to obtain the RC flux only in six cases. For the remaining events, the ribbon areas and hence the RC flux were underestimated. The ribbon area (A_R, in units of 10^{19} cm^2), the average magnetic field strength (B_R in units of Gauss), and the RC flux from the ribbon method are listed in columns 10, 11, and 12, respectively. When we searched for ribbon observations in TRACE 1600 Å data, we found eight events (events 19, 21, 32, 43, 45, 46, 49, and 53 noted with a superscript "T" in column 10). For event 43 there was only one frame in the rise phase, therefore the ribbon area is an underestimate. The remaining seven events had usable TRACE data. In column 10, the source of the ribbon data (H – Hα; T – TRACE) is noted. The poloidal flux Φ_p of MCs computed from the Lundquist solution (Lepping, Burlaga, and Jones, 1990) is listed in column 13. Of the many output parameters obtained by the flux rope fitting, we use the axial field strength (B_0) and the flux rope radius (R_0) at 1 AU to derive the poloidal flux of the MC,

$$\Phi_p = L(B_0 R_0)/x_{01}, \tag{2}$$

assuming that the flux rope extends up to the radius where the axial field component vanishes. Here x_{01} is the first zero (2.4048) of the Bessel function J_0 and L is the total length of the flux rope, taken as 2 AU following Nindos, Zhang, and Zhang (2003).

3. Analysis and Results

3.1. Comparison Between RC Flux from the Arcade and Ribbon Methods

We extend the case studies presented in Section 2.1 to all Cycle 23 eruptions that originated within ± 15° from the disk center and resulted in MCs at 1 AU (see Table 1). First we check whether the arcade and ribbon methods yield consistent results. To do this, we extracted the 15 events with ribbon information (Hα or TRACE) and listed them in Table 2. For six events, there were no usable ribbon data from either Hα or from TRACE 1600 Å (events 23, 24, 27, 39, 44, and 54 in Table 1). We separated Hα and TRACE data on ribbons along with the number of frames available for each event. We also list the number of frames available for each event in Hα and TRACE. In the last column, we list the name of the observatory that provided the Hα images. When the number of frames was insufficient to make complete ribbon measurements in an event, we considered the computed RC flux be an underestimate. Only three events (events 32, 49 and 53) had data both in Hα and TRACE. Table 2 shows that there were only a total of ten events with RC flux computed from flare ribbons. In the remaining five events, ribbons were observed, but not in a sufficiently large number of frames to compute the cumulative ribbon areas. However, we used these events to show that they provide lower limits to the RC flux and check whether they have the correct trend.

The RC fluxes from the arcade and ribbon methods are shown in Figure 4a as a scatter plot, indicating a high correlation ($r = 0.94$). A least-squares fit gives the regression equation,

$$\Phi_{rA} = 1.24(\Phi_{rR})^{0.99}. \tag{3}$$

Table 2 List of events with RC flux computed from Hα or TRACE 1600 Å ribbons.

ID	CME Date UT	Φ_{rA}	FrH	A_{RH}	$\langle B_{RH} \rangle$	Φ_{rRH}	FrT	A_{RT}	$\langle B_{RT} \rangle$	Φ_{rRT}	Hα
02	SOL1997-05-12T05:30	2.36	6	1.70	171.5	1.46	–	–	–	–	HIDA
09	SOL1999-04-13T03:30	1.46	1	2.06	46.8	0.48[b]	–	–	–	–	NAOJ
16	SOL2000-02-17T21:30	2.99	4	3.24	138.6	2.25	–	–	–	–	MLSO
19	SOL2000-07-14T10:54	13.10	1	1.69[a]	557.5	9.44[b]	71	5.64	446.9	12.61	MEUDON
21	SOL2000-07-25T02:43	1.13	–	–	–	–	29	0.82	310.3	1.27	–
26	SOL2000-10-09T23:50	5.10	1	3.08	125.1	1.93[b]	–	–	–	–	NAOJ
32	SOL2001-04-10T05:30	7.15	14	4.93	317.5	7.82	200	4.67	306.9	7.17	HIDA
33	SOL2001-04-26T12:30	12.00	9	3.86[a]	167.2	6.45[b]	–	–	–	–	OAFA
36	SOL2002-03-15T23:06	11.45	1	1.18[a]	363.1	4.28[b]	–	–	–	–	YNAO
37	SOL2002-04-15T03:50	10.80	11	0.81	1137.1	4.58	–	–	–	–	HIDA

Table 2 (*Continued*)

ID	CME Date UT	Φ_{rA}	FrH	A_{RH}	$\langle B_{RH}\rangle$	Φ_{rRH}	FrT	A_{RT}	$\langle B_{RT}\rangle$	Φ_{rRT}	Hα
43	SOL2002-07-29T12:07	6.15	–	–	–	–	8	0.64	426.4	1.35^b	–
45	SOL2003-10-28T11:30	20.75	–	–	–	–	62	7.05	592.1	20.88	–
46	SOL2003-10-29T20:54	21.60	3	2.21	540.9	5.99^b	101	3.96	698.4	13.82	MLSO
49	SOL2004-11-06T02:06	6.70	7	0.92	893.5	4.11	345	0.43	1168.8	2.52	HIDA
53	SOL2005-05-13T17:12	6.70	4	3.21	372.7	5.98	454	2.89	371.5	5.36	BBSO

Notes.

Φ_{rA} – RC flux (in 10^{21} Mx) obtained from the arcade method (half of the flux passing through area A_a).

FrH – Number of Hα frames available for measuring the RC flux.

A_{RH} – Cumulative ribbon area (in 10^{19} cm^2) from Hα observations. Superscript a denotes that only one of the ribbons in the pair was considered for flux measurement.

$\langle B_{RH}\rangle$ – Average magnetic field strength (G) within the cumulative Hα ribbon area.

Φ_{rRH} – RC flux (in 10^{21} Mx) in units of obtained from Hα ribbons. Suffix b stands for incomplete events.

Events without data during flare impulsive phase are considered incomplete.

FrT – Number of TRACE 1600 Å frames available for measuring the RC flux.

A_{RT} – Cumulative ribbon area from TRACE 1600 Å observations in 10^{19} cm^2.

$\langle B_{RT}\rangle$ – Average magnetic field strength (G) within the cumulative TRACE 1600 Å ribbon area.

Φ_{rRT} – RC flux (in 10^{21} Mx) in units of obtained from TRACE ribbons. Superscript b denotes that the RC flux is an underestimate due to lack of sufficient observations.

BBSO – Big Bear Solar Observatory (http://www.bbso.njit.edu/Research/FDHA/).

HIDA – Hida Observatory, Kyoto University (http://www.kwasan.kyoto-u.ac.jp/observation/data/index_en.html).

MEUDON – Observatory de Paris, Meudon (http://bass2000.obspm.fr/home.php).

MLSO – Mauna Loa Solar Observatory (http://www2.hao.ucar.edu/mlso/mlso-home-page).

NAOJ – Solar Observatory, NAOJ (http://solarwww.mtk.nao.ac.jp/en/database.html).

OAFA – Observatorio Astronomico Felix Aguilar (http://www.oafa.fcefn.unsj-cuim.edu.ar/hasta/Web/hastasearch.html).

YNAO – Yunnan Astronomical Observatory (http://swrl.njit.edu/ghn_web/latestimg/latestimg.php).

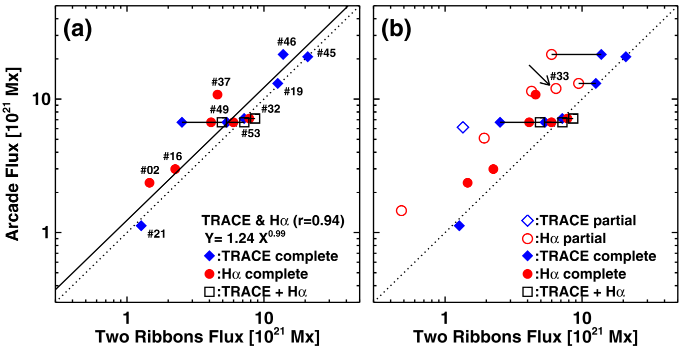

Figure 4 (a) Scatter plot between the RC fluxes obtained from the arcade method and the ribbon method for ten events identified by the event numbers. The RC flux from Hα ribbons (red symbols) and TRACE 1600 Å ribbons (blue symbols) are distinguished. Data points connected by a horizontal line represent ribbon measurements from Hα and TRACE. In these cases, the TRACE and Hα data were combined to obtain the cumulative area, and the resulting flux is indicated by a black square (events 32, 49, and 53). The dotted line corresponds to equal arcade and ribbon fluxes. The solid line is the least-squares fit to the data points (Hα + TRACE 1600 Å). The correlation coefficient (0.94) is higher than the critical value (0.549) of the Pearson correlation coefficient for ten data points at 95% confidence level. In events with both Hα and TRACE measurements, the combined flux (black squares) is used in the correlation. (b) The same scatter plot, but this time, it includes events with incomplete ribbon data (open circles and diamonds). The plotted fluxes are lower limits for these events. Event 33 discussed in the text is pointed at by an arrow.

This result is significant because it shows that the simpler arcade method works well. The regression line deviates only slightly from the equal-flux line ($\Phi_{rA} = \Phi_{rR}$). The largest deviation is for event 37, in which Φ_{rA} is greater than Φ_{rR} by a factor of ~ 2.4. In Figure 4b we include events that did not have complete ribbon information (open symbols). The RC fluxes from the ribbon method are underestimated in these events because not enough frames are available. However, the open symbols are consistent with the trend that the RC flux from the arcade method correlates with that from the ribbon method. If these events had complete observations, the open symbols would move closer to the equal-flux line. We also note that five of the ten data points in Figure 4a are on the line of equal fluxes. The fact that the equal-flux line needs to be multiplied by 1.24 to obtain the regression line indicates that the RC flux is overestimated by the arcade method and underestimated by the ribbon method, or both. Possibilities for the overestimate of the RC flux from the arcade method include i) the arcade is observed in the corona, resulting in a slight overestimate of the arcade area compared to the actual area at the photospheric level and hence a higher RC flux, and ii) the arcade flux might include contributions from very close to the neutral line, while the ribbons may start from a finite distance from the neutral line. These fluxes that do not participate in the flare reconnection can also contribute to an overestimate of the arcade flux.

Event 37 had 11 Hα frames covering most of the flare duration. There was no data coverage for the last 2 hours in the decay phase of the flare. Most likely, the RC flux from the ribbon method was underestimated. Except for this event, we see from Table 2 that the ratio Φ_{rA}/Φ_{rR} is in the range 0.89 to 1.6 for all events with well-defined Φ_{rR}. One of the events with the highest ratio (~ 1.6) is the 29 October 2003 eruption (event 46). This well-known eruption is from AR 10486 that resulted in a magnetic cloud (Gopalswamy *et al.*, 2005). Figure 5 shows an overview of the event with the EUV arcade and the PIL involved. The ribbon on the positive side was fragmented because of a narrow lane of negative field region at the northern end of the arcade. We used the ribbon on the negative side of the PIL, which was not fragmented. The times of the available Hα and TRACE 1600 Å frames are

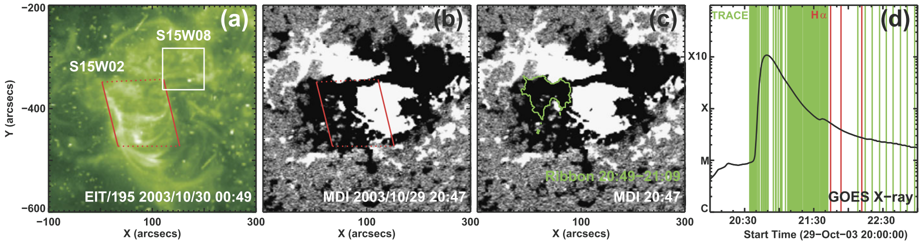

Figure 5 The 29 October 2003 eruption (event 46) that showed a large deviation between RC fluxes from the arcade and ribbon methods for the group of ten cases in which Φ_{rR} could be estimated. (a) PEA at 00:49 UT on 30 October 2003 with the edges of the arcade marked by the red lines. The white box placed at S15W08 marks the area where another flare occurred, but it did not affect the flux computations. (b) The arcade area superposed on an MDI magnetogram taken at 20:47 UT. (c) The combined ribbon area superposed on the MDI magnetogram. (d) The GOES soft X-ray light curve (black) with the times of TRACE (green) and Hα (red) images used in computing the ribbon areas. The second flare can be seen as a small increase in the GOES intensity around 21:30 UT. The main part of the flare had high-cadence TRACE observations, while in the late-decay phase the cadence dropped to below 10 min. Only three Hα images were available for this event.

marked in the GOES soft X-ray plot in Figure 5; these frames were used to compute the RC flux using the ribbon method. The early part of the flare ribbons was observed with high cadence, while the late-decay phase was observed with lower cadence by TRACE. In Hα, there were only three frames in the decay phase. Using the TRACE observations alone, we obtained an RC flux of $\sim 13.82 \times 10^{21}$ Mx. The Hα observation alone gave a lower value (5.99×10^{21} Mx) because of the incomplete observations. On the other hand, the Φ_{rA} of this event was 21.6×10^{21} Mx. It seems unlikely that Φ_{rA} in this event is overestimated. An underestimate of the RC flux using the ribbon method is possible because of the uneven coverage. For example, there was a gap of ~ 30 min between the last TRACE observation and the first Hα observation. Figure 5 also shows that the arcade extends farther to the south than the cumulative ribbon area, suggesting a possible underestimate of the RC flux. This shows that using the ribbon method can be subjective because it depends on the threshold used in defining the ribbons. The Halloween event on 28 October 2003 (event 45) was also an event in the list of Qiu *et al.* (2007), who estimated the RC flux from TRACE ribbons as 18.8×10^{21} Mx, which is similar to our value (20.88×10^{21} Mx). Both values are in good agreement with the RC flux from the arcade method.

The event on 26 April 2001 (event 33) was a clear case of an overestimated arcade flux; it is marked in Figure 4b. A large bipolar active region was located near the PIL of the arcade, but did not participate in the flare reconnection and hence contributed to overestimating Φ_{rA}. We estimate the unsigned flux that is due to the bipole as $\sim 15.2 \times 10^{21}$ Mx from the MDI magnetogram. Since the bipole did not participate in the eruption process, it needs to be subtracted from the total arcade flux (39.2×10^{21} Mx). The corrected arcade flux is 24.0×10^{21} Mx, and the RC flux accordingly is 12.0×10^{21} Mx. The corrected value is now closer to the equal-flux line. Unfortunately, there were Hα frames only in the decay phase of the flare, so the RC flux is underestimated. Using the nine available frames, the RC flux from the ribbon method was estimated as 6.45×10^{21} Mx. The true value is expected to be higher, therefore the data point will move to the right, closer to the equal fluxes line. This event demonstrates that large deviations can be understood by examining the magnetograms and the PEAs.

Qiu *et al.* (2007) may have misidentified the solar eruption in this event as described in Figure 6, which shows the PEA and the source region of the eruption from the *Yohkoh/Soft*

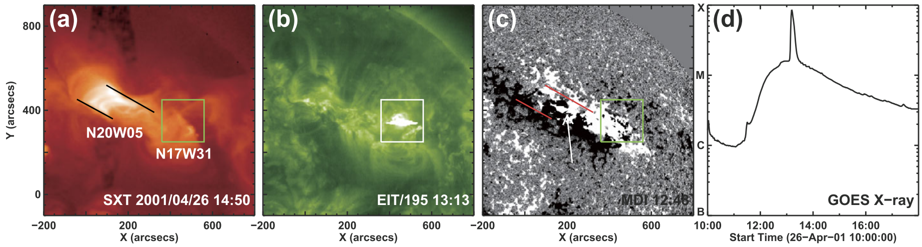

Figure 6 (a) A *Yohkoh*/*Soft X-ray Telescope* (SXT) image showing the PEA associated with the 26 April 2001 (event 33) eruption. The arcade was associated with the M1.5 gradual flare from N20W05. There was another impulsive flare starting around 13:04 UT, but to the west at N17W31 (inside the box shown). The full-disk SXT images did not capture the impulsive event, but the *SOHO*/EIT image shows the compact event at 13:13 UT enclosed by the box in (b). (c) MDI magnetogram of the extended magnetic region that hosted both the gradual and the impulsive eruptions. NOAA AR 9433 (pointed at by arrow) was located between the two eruptions, but did not participate in the eruption. The feet of the arcade (red lines) and the box within which the impulsive flare occurred are superposed on the magnetogram. (d) The GOES soft X-ray light curve showing the gradual M1.5 flare and the impulsive M8.9 flare.

X-ray Telescope, SOHO/EIT, MDI magnetogram, and the GOES light curve. This event has large uncertainties both at the Sun and at 1 AU. The CME of interest was a halo (likely to reach Earth) and first appeared in the LASCO FOV at 12:30 UT on 26 April 2001. The CME was associated with a gradual flare with a soft X-ray flare class of M1.5 that resulted in a large PEA. The centroid of the arcade was at N20W05. Roughly after the peak of the M1.5 gradual flare, an impulsive flare (M8.9) started at $\sim$13:04 UT and peaked at 13:13 UT. The M8.9 flare originated about 26° to the west of the centroid of the arcade. The M8.9 flare was not associated with the halo CME. It was associated with a narrow CME that first appeared in the LASCO FOV at 13:31 UT and was heading to the west. Qiu *et al.* (2007) used this flare to derive the flare RC flux, but it is unlikely that the 13:31 UT CME would have arrived at Earth. Both the M1.5 and M8.9 eruptions were from the same magnetic complex, which consisted of AR 9433 surrounded by weaker magnetic flux regions. Figure 6 shows that AR 9433 was located between the arcade centroid and the impulsive flare source. AR 9433 was located below the PEA, but close to its western part. The RC flux from the impulsive source was reported by Qiu *et al.* (2007) as 0.7×10^{21} Mx, more than an order of magnitude smaller than that of the M1.5 gradual flare (12.0×10^{21} Mx after eliminating the flux due to AR 9433).

A similar case of multiple events was observed on 11 April 2004 (event 49). At the solar source (AR 10696), three M-class flares occurred in quick succession (see http://www.lmsal.com/solarsoft/last_events_20041106_1019/index.html for details). The first was an M9.3 impulsive flare (00:11 to 00:42 UT) from N08E05 with no obvious CME association. The second was an M5.9 flare (00:44 to 01:10 UT) that occurred almost in the same location (N10E06) as the first, but was associated with a halo CME (Gopalswamy, Yashiro, and Akiyama, 2006, their Figure 4) with a speed of $\sim$818 km s^{-1} appearing at 01:31 UT in the LASCO FOV. The third flare was of X-ray class M3.6 (01:40 to 02:08 UT) and occurred to the west and south of the previous flares, at N07E00. This flare was associated with a faster (1111 km s^{-1}) partial-halo CME, which appeared at 02:06 UT in the LASCO FOV. It quickly caught up with the previous CME. The 1 AU MC has been determined to be due to the second CME (Gopalswamy *et al.*, 2010). Although the arcade appears to be a single one, it is possible to separate it into individual sections by looking at the time evolution. The arcade corresponding to the second CME had an RC flux of 6.70×10^{21} Mx, while the combined arcade yielded a flux of 14.85×10^{21} Mx. Both Hα and TRACE observations were

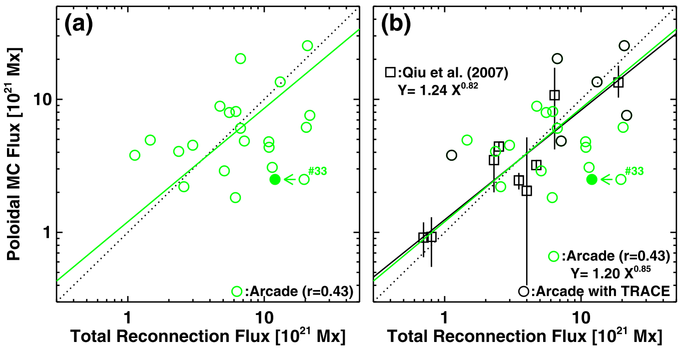

Figure 7 (a) Scatter plot between the RC flux from the arcade method (Φ_r) and the 1 AU poloidal flux (Φ_P) in the associated magnetic cloud. The dotted line denotes equal fluxes ($\Phi_P = \Phi_r$). The correlation coefficient $r = 0.43$ is higher than the critical value of the Pearson correlation coefficient (0.378 at 95% confidence level). (b) Same as (a) with the data points from Qiu *et al.* (2007) superposed (black squares), showing that the two sets of data yield a similar relation between Φ_r and Φ_P. The vertical black lines indicate the range of values over which the average flux was computed in Qiu *et al.* (2007). We have shown event 33 with the uncorrected (open circle) and corrected (filled circle) fluxes. Although this event follows the trend of the scatter plot, we did not include it for the reasons given in the text.

available for this event, which yielded reasonable values of the RC flux, especially when the two sets of observations were combined (see Figure 4a).

3.2. Comparison Between the RC Flux and the MC Poloidal Flux

We now consider how the RC flux from the arcade method relates to the poloidal flux of the associated MCs listed in Table 1. Figure 7a shows a scatter plot between Φ_r and Φ_P (we drop the subscript "A" in Φ_{rA} for simplicity). We see a modest correlation, with an equal number of data points on either side of the equal-flux ($\Phi_r = \Phi_P$) line. A linear least-squares fit to Φ_r–Φ_P pairs (on a logarithmic scale) gives the regression equation,

$$\Phi_P = 1.20(\Phi_r)^{0.85}. \tag{4}$$

The correlation coefficient ($r = 0.43$) is higher than the critical value for the Pearson correlation (0.378 at 95% confidence level). Thus the Φ_P–Φ_r relationship is very similar to Equation (1), obtained by Qiu *et al.* (2007) for nine events. The coefficient of Φ_r in Equation (4) is only 7.1% higher than that in Equation (1). Similarly, the exponent of Φ_r is only 3.6% larger than that in Qiu *et al.* (2007) result. More importantly, the RC flux used in Equation (1) was from the ribbon method, whereas it is from the arcade method in Equation (4). Thus we confirm the result presented in Figure 4, *viz.*, the RC fluxes obtained from the arcade and ribbon methods lead to similar correlation with the MC poloidal flux. In addition, we see that the flare RC flux at the Sun is closely related to the poloidal flux of the associated MC, especially close to the $\Phi_r = \Phi_P$ line. Webb *et al.* (2000) considered the axial flux of the MC and related it to the flux in the dimming region for event #2 and found good agreement. Axial field is related to, but smaller than, the poloidal flux in a force-free flux rope. These authors obtained a dimming flux of $\sim 1.0 \times 10^{21}$ Mx, which is smaller than the RC flux (see Table 1).

The close correspondence between the results of Qiu *et al.* (2007) and our result may be due to a combination of several circumstances. Since Qiu *et al.* used a flux rope length of

1 AU instead of the 2 AU used by us, we may be overestimating Φ_P. If we also overestimated the RC flux in the arcade method, then these two might have balanced to yield the same relationship between Φ_P and Φ_r. However, Qiu *et al.* (2007) used Φ_P values that are taken from three different sources. Sometimes the values differed by an order of magnitude for a given event. Therefore, the comparison between our Φ_P and that of Qiu *et al.* (2007) may not be appropriate. When we checked our Φ_P values with those in Qiu *et al.* (2007) for five events that are also in our list (events 21, 23, 32, 45, and 53), we found that our values are only slightly higher, by a factor 1.3. The reconnection flux from the ribbon method obtained by Qiu *et al.* (2007) in three of the five cases was lower than our reconnection flux from the ribbon method. Therefore it is possible that this underestimate and their use of 1 AU for the flux rope length balanced out. We also found that one of the data points (10 April 2001) differs between their Table 4 and their Figure 8c. When we used their table values, we obtained a new line with the same exponent, but with a slightly higher coefficient (1.24 *vs.* 1.12). Because of the small sample available for comparison, it is difficult to derive strong conclusions on the similarity between Equations (1) and (4).

It must be noted that sometimes the association between the solar and interplanetary events may be incorrect. For instance, in the case of the 10 April 2001 event (event 33) discussed in Section 3.1, the low value of the RC flux obtained by Qiu *et al.* (2007) matched the MC poloidal flux at 1 AU (1.25×10^{21} Mx). This is fortuitous because the CME–MC association was not correct. Moreover, the MC was quite complex, with different authors giving different durations ranging from 11 to 60 hours (see Table 1 of Qiu *et al.*, 2007). In the CDAW list, the MC was reported to have a duration of $\sim$11 hours. However, there was ICME material with a low proton temperature before and after the MC interval. Our poloidal flux value was 2.5×10^{21} Mx (since we use a flux rope length of 2 AU), which is lower by a factor of 4.8 than the RC flux from the arcade. Because of the uncertainties surrounding the 26 April 2001 event, we did not include it in the correlation, although the data points shown in Figure 7 are consistent with the rest of the events.

4. Discussion

We presented a new method to estimate the flare RC flux based on post-eruption arcades and the photospheric magnetic field underlying the arcades. We have shown that i) half the magnetic flux below post-eruption arcades is a reasonable representation of the flare RC flux (Figure 4), and ii) the RC flux obtained from the arcade method and the poloidal flux of the associated magnetic cloud at 1 AU are correlated significantly (Figure 7). The relationship is very similar to the one obtained by Qiu *et al.* (2007).

One of the major advantages of the new method is that it requires only one image that shows the "mature" arcade in EUV, X-rays, or even microwaves (see *e.g.*, Hanaoka *et al.*, 1994; Gopalswamy *et al.*, 2013a). Typically, this image corresponds to the decay phase of flares. Observations of post-eruption arcades are generally better available than that of flare ribbons. We see that only ten of the 23 eruptions from Cycle 23 had usable ribbon observations (from Hα and TRACE 1600 Å). On the other hand, 21 of the 23 eruptions had usable arcade observations. Thus $\sim$3 times more events are usable for the arcade method than for the ribbon method in Cycle 23. The reliability of the arcade method is important for space weather applications.

Hu *et al.* (2014) extended the study of Qiu *et al.* (2007) to include ten more events from Cycle 24, thus doubling their sample. They did find the continued correlation between the flare RC flux and MC poloidal flux, but with a pronounced deviation from the equal-flux line. Their sample size (19) is now similar to ours (21), but their solar source locations do not meet our longitude criterion (within $\pm 15°$) for all but two events. One of the two events did not have a computed RC flux. The only event matching our criterion (23 May 2010 eruption from N19W12) was reported to have $\Phi_r = 0.3 \times 10^{21}$ Mx and $\Phi_P = 0.83 \times 10^{21}$ Mx (Hu *et al.*, 2014). Substituting this Φ_r into Equation (4), we obtain $\Phi_P = 0.43 \times 10^{21}$ Mx, which is within a factor of two from Hu *et al.*'s (2014) Φ_P value. We note that Hu *et al.* (2014) considered only the Grad–Shafranov (GS) method of flux rope fitting rather than the force-free (FF) fitting we used. In Table 4 of Qiu *et al.* (2007), all the poloidal flux values from the FF method were higher than those from the GS method – by a factor of ~ 1.6 on average. In our case, we were able to estimate the poloidal flux using the GS method for 13 of the 21 events (Möstl 2014, private communication). In all 13 cases, the FF method gave a poloidal flux higher by a factor of five on average. Similar differences were also found in the five events in Qiu *et al.* (2007) that overlapped with ours: the GS fluxes were lower by factors of 5.8 than the Qiu *et al.* FF values and by a factor of 7.6 than our values. Since we have good information on magnetic clouds of Cycle 24 (Gopalswamy *et al.*, 2015), we will add more data points to the current 21 for better statistics and report the results elsewhere.

We considered only eruptions from the disk center that were observed as MCs at 1 AU. However, there are many disk-center eruptions that are not observed as MCs. Propagation effects such as deflection in the corona (Xie, Gopalswamy, and St. Cyr, 2013; Mäkelä *et al.*, 2013) seem to be responsible for the non-cloud appearance of these events at 1 AU, even though there is no difference in the source properties of cloud and non-cloud ICMEs (Gopalswamy *et al.*, 2013a; Yashiro *et al.*, 2013). Therefore, it is possible to estimate the expected poloidal flux of the non-cloud ICMEs at 1 AU from the RC flux. Marubashi *et al.* (2015) were able to fit a flux rope to all but three of the non-cloud ICMEs in the CDAW list. A comparison between the RC flux and the poloidal flux from Marubashi *et al.* (2015) may provide a clue to understand why the Lepping, Burlaga, and Jones (1990) force-free fitting did not recognize flux rope signatures.

5. Summary and Conclusions

We investigated a set of 21 solar eruptions originating from within $\pm 15°$ of the disk center and the associated magnetic clouds from Solar Cycle 23 to demonstrate a new method of measuring the flare RC flux. We measured the RC flux by combining observations of post-eruption arcades in EUV and line-of-sight photospheric magnetic fields. We also measured the RC flux from Hα and TRACE 1600 Å observations using the flare ribbon method. We found that the RC flux obtained from the two methods agreed quite closely. The RC flux from the arcade method is slightly higher than the flux from the ribbon method. This is mostly due to insufficient flare ribbon data. Occasionally, there may be high flux close to the polarity inversion line that does not participate in the reconnection and hence can cause an overestimate of the arcade RC flux. We also computed the poloidal flux of the associated magnetic clouds at 1 AU and found it to be approximately equal to the RC flux. This result is consistent with the idea that the flux ropes are formed during eruptions and any pre-existing flux rope needs to be rather small in the set of events we considered.

Acknowledgements We thank the ACE, Wind and SOHO teams for providing the data on line. SOHO is a project of international collaboration between ESA and NASA. We thank C. Möstl for providing the poloidal flux of 13 magnetic clouds using the Grad–Shafranov method. Our work was supported by NASA's Living with a Star Program.

Disclosure of Potential Conflicts of Interest The authors declare that they have no conflicts of interest.

References

Aschwanden, M.J., Alexander, D.: 2001, Flare plasma cooling from 30 MK down to 1 MK modeled from Yohkoh, GOES, and TRACE observations during the Bastille Day Event (14 July 2000). *Solar Phys.* **204**, 91. DOI.

Baker, D.N., Pulkkinen, T.I., Li, X., Kanekal, S.G., Blake, J.B., Selesnick, R.S., *et al.*: 1998, A strong CME-related magnetic cloud interaction with the Earth's Magnetosphere: ISTP observations of rapid relativistic electron acceleration on May 15, 1997. *Geophys. Res. Lett.* **29**, 2975. DOI.

Brueckner, G.E., Howard, R.A., Koomen, M.J., Korendyke, C.M., Michels, D.J., Moses, J.D., *et al.*: 1995, The Large Angle Spectroscopic Coronagraph (LASCO). *Solar Phys.* **162**, 357. DOI.

Burlaga, L., Sittler, E., Mariani, F., Schwenn, R.: 1981, Magnetic loop behind an interplanetary shock – Voyager, Helios, and IMP 8 observations. *J. Geophys. Res.* **86**, 6673. DOI.

Delaboudiniére, J.-P., Artzner, G.E., Brunaud, J., Gabriel, A.H., Hochedez, J.F., Millier, F., *et al.*: 1995, EIT: Extreme-Ultraviolet Imaging Telescope for the SOHO mission. *Solar Phys.* **162**, 291. DOI.

Domingo, V., Fleck, B., Poland, A.I.: 1995, The SOHO mission: An overview. *Solar Phys.* **162**, 1. DOI.

Gibson, S.E., Fan, Y., Török, T., Kliem, B.: 2006, The evolving sigmoid: Evidence for magnetic flux ropes in the corona before, during, and after CMEs. *Space Sci. Rev.* **124**, 131. DOI.

Gopalswamy, N.: 2009, Coronal mass ejections and space weather. In: Tsuda, T., Fujii, R., Shibata, K., Geller, M.A. (eds.) *Climate and Weather of the Sun Earth System (CAWSES): Selected Papers from the 2007 Kyoto Symposium*, Terrapub, Tokyo, 77.

Gopalswamy, N., Yashiro, S., Akiyama, S.: 2006, Coronal mass ejections and space weather due to extreme events. In: Gopalswamy, N., Bhattacharyya, A. (eds.) *Solar Influence on the Heliosphere and Earth's Environment: Recent Progress and Prospects*, Quest Publications, Mumbai, 79.

Gopalswamy, N., Yashiro, S., Krucker, S., Stenborg, G., Howard, R.A.: 2004, Intensity variation of large solar energetic particle events associated with coronal mass ejections. *J. Geophys. Res.* **109**, A12105. DOI.

Gopalswamy, N., Yashiro, S., Liu, Y., Michalek, G., Vourlidas, A., Kaiser, M.L., Howard, R.A.: 2005, Coronal mass ejections and other extreme characteristics of the 2003 October–November solar eruptions. *J. Geophys. Res.* **110**, A09S15. DOI.

Gopalswamy, N., Xie, H., Mäkelä, P., Akiyama, S., Yashiro, S., Kaiser, M.L., Howard, R.A., Bougeret, J.-L.: 2010, Interplanetary shocks lacking type II radio bursts. *Astrophys. J.* **710**, 1111. DOI.

Gopalswamy, N., Xie, H., Yashiro, S., Akiyama, S., Mäkelä, P., Usoskin, I.G.: 2012, Properties of ground level enhancement events and the associated solar eruptions during solar cycle 23. *Space Sci. Rev.* **171**, 23. DOI.

Gopalswamy, N., Mäkelä, P., Akiyama, S., Xie, H., Yashiro, S., Reinard, A.A.: 2013a, The solar connection of enhanced heavy ion charge states in the interplanetary medium: Implications for the flux-rope structure of CMEs. *Solar Phys.* **284**, 17. DOI.

Gopalswamy, N., Nieves-Chinchilla, T., Hidalgo, M., Zhang, J., Riley, P., van Driel-Gesztelyi, L., Mandrini, C.H.: 2013b, Preface *Solar Phys.* **284**, 1. DOI.

Gopalswamy, N., Yashiro, S., Xie, H., Akiyama, S., Mäkelä, P.: 2015, Properties and geoeffectiveness of magnetic clouds during solar cycles 23 and 24. *J. Geophys. Res.* **120**, 9221. DOI.

Hanaoka, Y., Kurokawa, H., Enome, S., Nakajima, H., Shibasaki, K., Nishio, M., *et al.*: 1994, Simultaneous observations of a prominence eruption followed by a coronal arcade formation in radio, soft X-rays, and H(alpha). *Publ. Astron. Soc. Japan* **46**, 205.

Hu, Q., Qiu, J., Dasgupta, B., Khare, A., Webb, G.M.: 2014, Structures of interplanetary magnetic flux ropes and comparison with their solar sources. *Astrophys. J.* **793**, 53. DOI.

Leamon, R.J., Canfield, R.C., Jones, S.L., Lambkin, K., Lundberg, B.J., Pevtsov, A.A.: 2004, Helicity of magnetic clouds and their associated active regions. *J. Geophys. Res.* **109**, A05106. DOI.

Lepping, R.P., Burlaga, L.F., Jones, J.A.: 1990, Magnetic field structure of interplanetary magnetic clouds at 1 AU. *J. Geophys. Res.* **95**, 11957. DOI.

Lepri, S.T., Zurbuchen, T.H., Fisk, L.A., Richardson, I.G., Cane, H.V., Gloeckler, G.: 2001, Iron charge state distributions as an identifier of interplanetary coronal mass ejections. *J. Geophys. Res.* **106**, 29231. DOI.

Lin, J., Raymond, J.C., van Ballegooijen, A.A.: 2004, The role of magnetic reconnection in the observable features of solar eruptions. *Astrophys. J.* **602**, 422. DOI.

Linton, M.G., Moldwin, M.B.: 2009, A comparison of the formation and evolution of magnetic flux ropes in solar coronal mass ejections and magnetotail plasmoids. *J. Geophys. Res.* **114**, A00B09. DOI.

Longcope, D.W., Beveridge, C.: 2007, Quantitative, topological model of reconnection and flux rope formation in a two-ribbon flare. *Astrophys. J.* **669**, 621. DOI.

Longcope, D., Beveridge, C., Qiu, J., Ravindra, B., Barnes, G., Dasso, S.: 2007, Modeling and measuring the flux reconnected and ejected by the two-ribbon flare/CME event on 7 November 2004. *Solar Phys.* **244**, 45. DOI.

Mäkelä, P., Gopalswamy, N., Xie, H., Mohamed, A.A., Akiyama, S., Yashiro, S.: 2013, Coronal hole influence on the observed structure of interplanetary CMEs. *Solar Phys.* **284**, 59. DOI.

Marubashi, K.: 1997, Interplanetary magnetic flux ropes and solar filaments. In: Crooker, N., Joselyn, J.A., Feynman, J. (eds.) *Coronal Mass Ejections*, *Geophysical Monograph Series* **99**, American Geophysical Union, Washington DC, 147. DOI.

Marubashi, K., Akiyama, S., Yashiro, S., Gopalswamy, N., Cho, K.-S., Park, Y.-D.: 2015, Geometrical relationship between interplanetary flux ropes and their solar sources. *Solar Phys.* **290**, 137. DOI.

Mewaldt, R.A., Looper, M.D., Cohen, C.M.S., Haggerty, D.K., Labrador, A.W., Leske, R.A., Mason, G.M., Mazur, J.E., von Rosenvinge, T.T., *et al.*: 2012, Energy spectra, composition, and other properties of ground-level events during solar cycle 23. *Space Sci. Rev.* **171**, 97. DOI.

Moore, R.L., Sterling, A.C., Suess, S.T.: 2007, The width of a solar coronal mass ejection and the source of the driving magnetic explosion: A test of the standard scenario for CME production. *Astrophys. J.* **668**, 1221. DOI.

Mouschovias, T.Ch., Poland, A.I.: 1978, Expansion and broadening of coronal loop transients – a theoretical explanation. *Astrophys. J.* **220**, 675. DOI.

Nakai, Y., Hattori, A.: 1985, Domeless solar tower telescope at the Hida Observatory. *Mem. Fac. Sci., Kyoto Univ.* **36**(3), 385.

Nindos, A., Zhang, J., Zhang, H.: 2003, The magnetic helicity budget of solar active regions and coronal mass ejections. *Astrophys. J.* **594**, 1033. DOI.

Qiu, J., Hu, Q., Howard, T.A., Yurchyshyn, V.B.: 2007, On the magnetic flux budget in low-corona magnetic reconnection and interplanetary coronal mass ejections. *Astrophys. J.* **659**, 758. DOI.

Reinard, A.A.: 2008, analysis of interplanetary coronal mass ejection parameters as a function of energetics, source location, and magnetic structure. *Astrophys. J.* **682**, 1289. DOI.

Reiner, M.J., Kaiser, M.L., Karlický, M., Jiřička, K., Bougeret, J.-L.: 2001, Bastille day event: A radio perspective. *Solar Phys.* **204**, 121. DOI.

Scherrer, P.H., Bogart, R.S., Bush, R.I., Hoeksema, J.T., Kosovichev, A.G., Schou, J., *et al.*: 1995, The solar oscillations investigation – Michelson Doppler Imager. *Solar Phys.* **162**, 129. DOI.

Strong, K., Bruner, M., Tarbell, T., Title, A., Wolfson, C.J.: 1994, Trace – the transition region and coronal explorer. *Space Sci. Rev.* **70**, 119. DOI.

Thompson, B.J., Plunkett, S.P., Gurman, J.B., Newmark, J.S., St. Cyr, O.C., Michels, D.J.: 1998, SOHO/EIT observations of an Earth-directed coronal mass ejection on May 12, 1997. *Geophys. Res. Lett.* **24**, 2465. DOI.

Titov, V.S., Mikic, Z., Linker, J.A., Lionello, R.: 2008, 1997 May 12 coronal mass ejection event. I. A simplified model of the preeruptive magnetic structure. *Astrophys. J.* **675**, 1614. DOI.

Webb, D.F., Lepping, R.P., Burlaga, L.F., DeForest, C.E., Larson, D.E., Martin, E.F., Plunkett, S.F., Rust, D.M.: 2000, The origin and development of the May 1997 magnetic cloud. *J. Geophys. Res.* **105**, 27251. DOI.

Xie, H., Gopalswamy, N., St. Cyr, O.C.: 2013, Near-Sun flux rope structure of CMEs. *Solar Phys.* **284**, 47. DOI.

Yan, Y., Huang, G.: 2003, Reconstructed 3-d magnetic field structure and hard X-ray two ribbons for 2000 Bastille-day event. *Space Sci. Rev.* **107**, 111. DOI.

Yashiro, S., Michalek, G., Akiyama, S., Gopalswamy, N., Howard, R.A.: 2008, Spatial relationship between solar flares and coronal mass ejections. *Astrophys. J.* **673**, 1174. DOI.

Yashiro, S., Gopalswamy, N., Mäkelä, P., Akiyama, S.: 2013, Post-eruption arcades and interplanetary coronal mass ejections. *Solar Phys.* **284**, 5. DOI.

Zhang, J., Dere, K.P.: 2006, A statistical study of main and residual accelerations of coronal mass ejections. *Astrophys. J.* **649**, 1100. DOI.

Zhang, J., Dere, K.P., Howard, R.A., Kundu, M.R., White, S.M.: 2001, On the temporal relationship between coronal mass ejections and flares. *Astrophys. J.* **559**, 452. DOI.

Zhang, J., Richardson, I.G., Webb, D.F., Gopalswamy, N., Huttunen, E., Kasper, J.C., *et al.*: 2007, Solar and interplanetary sources of major geomagnetic storms ($Dst <= -100$ nT) during 1996–2005. *J. Geophys. Res.* **112**, A10102. DOI.